

Estimating Bohm's quantum force using Bayesian statistics

Jeremy B. Maddox^{a)} and Eric R. Bittner^{b)}

Department of Chemistry, University of Houston, Houston, Texas 77204

(Received 28 April 2003; accepted 8 July 2003)

In this paper we develop an approximate methodology for estimating the multidimensional quantum density associated with a statistical bundle of de Broglie–Bohm trajectories. The quantum density is constructed as a discrete sum of nonequivalent Gaussian components. We incorporate the ideas of Bayesian statistical analysis and an expectation-maximization procedure to compute an approximate quantum force that drives the statistical ensemble quantum trajectories. © 2003 American Institute of Physics. [DOI: 10.1063/1.1604772]

I. INTRODUCTION

The fundamental objective in statistical analysis pertains to the development of probabilistic models that can explain and predict the observations of interesting physical processes. The capacity to estimate the effectiveness of a statistical model goes hand in hand with the ability to improve its explanatory and predictive powers. Problems related to this idea are encountered throughout the biological, physical, and social sciences. In some cases, it is possible to construct a model that incorporates prior knowledge and experience in terms of a few (or more often many!) adjustable parameters. The primary goal is then to find a particular set of parameters that best explains the observed data and can predict the likely outcome of new observations. The mathematical formalism which quantifies these notions is provided within the Bayesian construction of statistical analysis.¹ In the Bayesian approach, probabilities are treated subjectively as a degree of belief rather than a frequency of observation. Though this distinction is somewhat controversial, Bayesian statistics are crucially important to probabilistic learning,² decision making theory, and statistical inference problems. In the quantum physics literature, Bayesian probabilities have recently been addressed in connection with a diverse range of problems including many-body potential energy surfaces,^{3,4} the control of open quantum systems,⁵ quantum tomography,⁶ measurement theory in quantum logic devices,^{7–10} and quantum Monte Carlo simulations.^{11,12}

In the present paper we develop an approximate methodology for estimating the multidimensional quantum distribution function associated with a statistical ensemble of de Broglie–Bohm space-time trajectories. The scheme that we propose is built upon a parametrized Gaussian model for the quantum density. We explore the advantages and limitations of this model and outline an iterative procedure based upon Bayesian probability theory for finding a set of Gaussian parameters that mimics the true density function. This fitted density is then used to compute an approximate quantum force, that drives the ensemble of trajectories. We show how

this approach can be used to determine the ground-state density and energy of a multidimensional quantum-mechanical system.

The organization for the rest of this paper is as follows: In Sec. II we discuss quantum-mechanical paths and briefly review the key features of the de Broglie–Bohm interpretation of quantum mechanics. Section III introduces the mixture model^{13,14} approximation and expectation-maximization algorithm¹⁵ that are used to estimate the quantum density. In Sec. IV we present some benchmark calculations, which are representative of our methodology. Finally, Sec. V concludes.

II. THEORETICAL BACKGROUND

A. Classical versus quantum paths

According to Newton's second law, the physical motion of a particle is characterized by a space-time path $\mathbf{r}(t)$ that satisfies the equations of motion

$$\dot{\mathbf{r}}(t) = \mathbf{p}(t)/m, \quad (1)$$

$$\dot{\mathbf{p}}(t) = -\nabla V[\mathbf{r}(t)], \quad (2)$$

where m is the mass of the particle and $-\nabla V(\mathbf{r})$ is the force associated with an externally applied potential energy field. In principle, the position \mathbf{r} and momentum \mathbf{p} of a classical particle can be determined with arbitrary precision, and it is well known that exactly specifying the initial conditions $\mathbf{r}_0 = \mathbf{r}(0)$ and $\mathbf{p}_0 = \mathbf{p}(0)$ will completely determine the particle's trajectory for all time.

In quantum mechanics, however, the situation is quite different. The precision with which \mathbf{r} and \mathbf{p} can be simultaneously known is limited by Heisenberg's uncertainty principle: $\Delta\mathbf{r}\Delta\mathbf{p} \geq \hbar/2$. The dynamical properties of a particle are embodied in a complex wave function $\psi(\mathbf{r}, t)$ that satisfies the time-dependent Schrödinger equation

$$i\hbar \partial_t \psi(\mathbf{r}, t) = -\frac{\hbar^2}{2m} \nabla^2 \psi(\mathbf{r}, t) + V(\mathbf{r})\psi(\mathbf{r}, t). \quad (3)$$

Traditionally, the wave function is interpreted as a time-dependent amplitude associated with the instantaneous probability of finding the particle in an infinitesimal volume of

^{a)}Current address: Department of Chemistry, University of Rochester, Rochester New York 14627. Electronic mail: jmaddox@uh.edu

^{b)}Electronic mail: bittner@uh.edu

space $d^3\mathbf{r}$ about the point \mathbf{r} . From this point of view, individual physical particles are treated as statistical objects, and the notion that particles follow definite paths in space-time is apparently a meaningless concept in quantum mechanics.

One way to rationalize this disparity among the classical and quantum theories is due to the Feynman path integral approach to quantum mechanics.¹⁶ According to Feynman's analysis, a path $\mathbf{r}(t)$ connecting two points in space-time is associated with a complex phase factor $\phi = \exp(iS_{cl}/\hbar)$ determined by the classical action

$$S_{cl}[\mathbf{r}(t)] = \int_0^t ds \frac{1}{2} m \dot{\mathbf{r}}^2 - V(\mathbf{r}) \quad (4)$$

along the path. The probability amplitude with which a particle makes a transition from an initial point $(\mathbf{r}_0, 0)$ to some final point (\mathbf{r}_f, t) is expressed as the sum of phase factors over all possible paths connecting the two points. For a quantum-mechanical particle, no particular path is preferred; therefore we must consider an infinite number of paths in order to compute the transition probability. For macroscopic objects, however, the classical action is much larger than \hbar , implying that the net contribution of phase in the transition amplitude is due to the path that minimizes the classical action. Hence the most probable path for a macroscopic object will be a trajectory that also satisfies the classical equations of motion. Feynman's treatment is particularly enlightening because it allows us to discuss both classical and quantum-mechanical phenomena on an equal footing, that is, in terms of an ensemble of all possible paths that effectively reduces to the classical trajectory in the limit that \hbar is small.

B. de Broglie–Bohm interpretation

Another formulation of quantum mechanics in terms of an ensemble of paths is due to the work of de Broglie^{17–19} and Bohm.^{20–23} In the de Broglie–Bohm interpretation of quantum mechanics one assumes that a quantum-mechanical system is physically composed of two parts: a wave *and* a point particle. Mathematically, the wave is represented by a wave function $\psi(\mathbf{r}, t)$ that satisfies Eq. (3) and is associated with the probability density $\rho(\mathbf{r}, t) = |\psi(\mathbf{r}, t)|^2$ for finding the particle when its exact position is unknown. Regardless of whether or not it can be observed, the particle always follows a precisely defined trajectory. The wave function plays a direct physical role in this by influencing the particle's trajectory through the introduction of a nonlocal “quantum potential” that gives rise to all nonclassical behavior including zero-point energy, tunneling, and self-interference effects.

To see this influence, we begin by writing the wave function in complex polar form

$$\psi(\mathbf{r}, t) = \rho(\mathbf{r}, t)^{1/2} \exp[iS(\mathbf{r}, t)/\hbar], \quad (5)$$

where the density $\rho(\mathbf{r}, t)$ and phase $S(\mathbf{r}, t)$ (quantum action) are real functions dependent upon space and time. The particle is assumed to follow a definite trajectory $\mathbf{r}(t)$ along which its velocity

$$\dot{\mathbf{r}} = \mathbf{v}(\mathbf{r}(t), t) = \nabla S(\mathbf{r}(t), t)/m \quad (6)$$

is determined by the phase amplitude of the wave function. For notational convenience we will drop the explicit dependence on \mathbf{r} and t . Substituting Eqs. (5) and (6) into Schrödinger's equation and equating the real and imaginary components, yields a pair of coupled partial differential equations

$$\partial_t \rho = -\nabla \cdot (\rho \mathbf{v}), \quad (7)$$

$$\partial_t S = -(Q + V) - \frac{1}{2} m \mathbf{v}^2, \quad (8)$$

which are easily identified as the continuity equation and a generalized Hamilton–Jacobi equation, respectively. The quantum potential term $Q = Q(\mathbf{r}, t)$, given by

$$Q = -\frac{\hbar^2}{4m} \left[\frac{\nabla^2 \rho}{\rho} - \frac{1}{2} \left(\frac{\nabla \rho}{\rho} \right)^2 \right], \quad (9)$$

distinguishes Eq. (8) from a purely classical equation and encapsulates the nonlocal influence of ψ on the trajectory of the particle. The quantum potential is often interpreted as an internal energy or “shape” energy associated with the curvature of the quantum density. We can explicitly include Q into the equations of motion for the particle by introducing a material time derivative

$$d_t f = \partial_t f + \mathbf{v} \cdot \nabla f \quad (10)$$

such that the field equations of motion for ρ and S are given by

$$d_t \rho = -\rho \nabla \cdot \mathbf{v}, \quad (11)$$

$$d_t S = \frac{1}{2} m \mathbf{v}^2 - (Q + V), \quad (12)$$

where the notation d_t signifies the time rate of change in the inertial reference frame of a particle moving along the trajectory $\mathbf{r}(t)$ with velocity $\mathbf{v}(\mathbf{r}(t), t)$. It is evident from the right-hand side of Eq. (12) that $d_t S$ represents a generalized Lagrangian $\mathcal{L}(\mathbf{r}(t), t)$ for the quantum-mechanical system. Taking $\nabla \mathcal{L}$, we have the relations

$$\dot{\mathbf{v}} = -\nabla(Q + V)/m, \quad (13)$$

$$\dot{\mathbf{r}} = \mathbf{v} = \nabla S/m, \quad (14)$$

which appear to be a quantum-mechanical analogue of Newton's equations that bears a quantum force term $F_Q = -\nabla Q$ supplementing the classical force. We make a special note here to emphasize that the fields ρ , S , \mathbf{v} , and all their derivatives in Eqs. (11)–(14) are implicitly evaluated along the path $\mathbf{r} = \mathbf{r}(t)$, and this path is the trajectory of a physically real point particle, at least within the de Broglie–Bohm paradigm.

C. Quantum hydrodynamic trajectories

It is fairly obvious from Eqs. (11)–(14) that if the wave function for a system were known, one would simply need to choose an initial position vector $\mathbf{r}(0)$ to completely specify the state of the system for all time. While this feature of the de Broglie–Bohm program is indeed a useful interpretive tool, we are still faced with the often formidable task of solving the time-dependent Schrödinger equation.

To remedy this situation, we begin by formally introducing an ensemble of quantum trajectories

$$\mathcal{R}(t) = \{\mathbf{r}_1(t), \dots, \mathbf{r}_n(t)\}, \quad (15)$$

which are distinguished from one another by their initial positions at time $t=0$. Just as one can construct a conceptual ensemble of fictitious fluid particles to represent a classical fluid, we have established an analogous ensemble of probability fluid elements to sustain the quantum density, phase, and velocity field. The theoretical groundwork for the evolution of these “particles” has already been laid out. One notable exception is that Eqs. (11) and (12) are now to be defined over a whole ensemble of quantum trajectories that simultaneously satisfy the set of differential equations given by

$$\dot{\mathbf{v}}_i = \nabla \mathcal{L}(\mathbf{r}_i(t), t), \quad (16)$$

$$\dot{\mathbf{r}}_i = \mathbf{v}_i. \quad (17)$$

Given an initial wave function $\psi(\mathbf{r}_i(0), 0)$ defined over the ensemble of points $\mathcal{R}(0)$, we can simultaneously solve Eqs. (11) and (12) to reconstruct the wave function at a later time t according to the relation

$$\begin{aligned} \psi(\mathbf{r}_i(t), t) = & \psi(\mathbf{r}_i(0), 0) \exp\left(-\frac{1}{2} \int_0^t \nabla \cdot \mathbf{v}(\mathbf{r}_i(s), s) ds\right) \\ & \times \exp\left(\frac{i}{\hbar} \int_0^t \mathcal{L}(\mathbf{r}_i(s), s) ds\right), \end{aligned} \quad (18)$$

where the wave function is represented point-wise along the ensemble of paths $\mathcal{R}(t)$. We emphasize that there is no approximation in Eq. (18), and it is a formal solution to the Schrödinger equation evaluated explicitly over a set of hydrodynamiclike quantum trajectories.

A few comments on the behavior of quantum trajectories are in order. First, the single-valuedness of $\psi(\mathbf{r}, t)$ requires that quantum trajectories must not intersect one another. If two trajectories were to cross, it would imply that the wave function has two distinct values of phase at the same point in space-time. Similarly, trajectories are not allowed to cross through nodal regions of the wave function where the phase is discontinuous and the probability of finding a particle is zero. This restriction is strictly upheld by the influence of the quantum force, which is very intense around nodal surfaces. Moreover, if the ensemble of trajectories are initially distributed according to the probability density $\rho(\mathbf{r}, 0)$, then the ensemble will be representative of $\rho(\mathbf{r}, t)$ for all time. This is simply a consequence of the statistical assumption on $\psi(\mathbf{r}, t)$ and is consistent with the continuity of quantum probability density. Finally, in the limit that $\hbar \rightarrow 0$, the ensemble equations of motion decouple, and the trajectories will evolve independently of one another according to Newton's equations.

In essence, the de Broglie–Bohm picture depicts a quantum-mechanical system in terms of an ensemble of correlated particle trajectories. Though the true particle follows a unique trajectory, it is inextricably coupled to an ensemble of alternate paths by the influence of the wave function acting through a quantum force.

D. Computational considerations

Numerical solutions of the time-dependent Schrödinger equation are traditionally obtained by calculating the short-time quantum propagator using fast Fourier transforms,²⁴ finite basis sets, or discrete variable representations.²⁵ Typically, the computational over-head associated with these techniques scales exponentially with the dimensionality of the physical problem. Trajectory-based methodologies, on the other hand, offer tremendous numerical scaling advantages, especially for high dimensional systems where traditional techniques are not feasible. In particular, the de Broglie–Bohm interpretation of quantum mechanics has inspired a growing number of theoretical and computational studies involving a wide range of problems such as reactive scattering dynamics,^{26,27} tunneling systems,^{28–31} mixed quantum/classical simulations,^{32–35} electronic transitions,^{36–38} photodissociation,^{39–42} mixed quantum states,^{43,44} and quantum dissipation.^{45–47}

The quantum trajectory method (QTM), developed by Wyatt and co-workers,^{26,28} incorporates the ideas of computational fluid dynamics to solve the hydrodynamic field equations over a discrete ensemble of quantum fluid elements. Using finite element methods, the fluid particles are arranged into small neighborhoods over which a moving weighted least squares (MWLS) fitting procedure⁴⁸ is used to locally expand the hydrodynamic fields ρ (more typically $\log \rho$), S , and \mathbf{v} in a simple polynomial basis. Once the fields and their derivatives are known, the integrals in Eq. (18) along with solutions to Eqs. (16) and (17) are evaluated over a short time step. While this strategy scales almost linearly with the number of trajectories, its versatility in practice is hindered by the fact that the ensemble of particles generally tends to become extremely disorganized for anharmonic systems making it difficult, if not impossible, to fit the quantum hydrodynamic fields. This becomes especially apparent around the nodes of the wave function, where the fitting errors will often times cause the quantum trajectories to cross one another leading to spurious numerical results. Very recently,^{49,50} new methods in adaptive grids have been developed to formulate a reconstruction of the wave function over an ensemble of generalized hydrodynamic trajectories that avoids the problem with quantum nodes and provides a much more stable framework for solving the hydrodynamic equations of motion.

Another application of the de Broglie–Bohm theory includes the development of semiclassical approximation strategies for including quantum effects into otherwise classical calculations. Garashchuk and Rassolov^{51,52} have recently presented a semiclassical methodology based upon de Broglie–Bohm trajectories that is formally insensitive to trajectory crossings and also avoids explicitly solving the continuity equation. In this approximate methodology, the quantum density is convoluted with a minimum uncertainty Gaussian wave packet and expanded in a linear combination of Gaussian functions

$$\rho(x) \approx f(x) = \sum_n c_n^2 \exp[-a_n^2(x - X_n)]. \quad (19)$$

The Gaussian parameters $s = \{c_n, X_n, a_n\}$ in Eq. (19) are determined by minimizing the functional

$$F = \int [\rho(x) - f(x)]^2 dx \quad (20)$$

using an iterative procedure which explicitly involves solving the set of equations $\partial F / \partial s_k = 0$. The parametrized density leads to an approximate quantum potential (AQP) that is used to propagate an ensemble of trajectories. Garashchuk and Rassolov have presented results for Eckart barrier tunneling that improve upon the Herman–Kluck semiclassical initial value representation (IVR) method⁵³ and are shown to agree quite well with exact quantum-mechanical results. A similar idea has also been explored by Donoso and Martens^{54–56} for propagating a correlated ensemble of quantum trajectories in phase space. Following Wigner's analysis,⁵⁷ quantum effects are introduced into the equations of motion by including a series of nonclassical force terms,

$$\dot{q} = p/m, \quad (21)$$

$$\dot{p} = -V'(q) + \sum_{k=1}^{\infty} \left(\frac{\hbar}{2i} \right)^{2k} \frac{\partial_q^{2k+1} V(q)}{(2k+1)!} \frac{\partial_p^{2k} \rho(q, p)}{\rho(q, p)}, \quad (22)$$

that give the quantum corrections to Hamilton's equations in increasing powers of \hbar . These terms involve higher-order spatial and momentum derivatives of the potential energy and probability distribution function, respectively. For systems where the potential surface has a finite number of non-zero derivatives the series in Eq. (22) truncates. Donoso and Martens have introduced a Gaussian ansatz to describe the instantaneous local structure of $\rho(q, p)$ about a trajectory. The phase space “quantum force” is evaluated in terms of Gaussian parameters which are computed by taking local moments of dynamical variables over the phase space ensemble. In the following section we present an approach based upon Bayesian statistical analysis for simulating the dynamics of a quantum-mechanical system by propagating an ensemble of trajectories with nonclassical forces.

III. DENSITY ESTIMATION

A. Mixture model

Suppose that $\mathcal{R} = \{\mathbf{r}_1, \dots, \mathbf{r}_N\}$ is an ensemble of de Broglie–Bohm fluid elements that statistically represents a multidimensional quantum probability density. Such a distribution of data points can be generated from a Metropolis sampling procedure or perhaps from the output of a quantum Monte Carlo simulation.^{58,59} In order to propagate these particles in time we must evaluate ρ and its derivatives for every member in the ensemble. Instead of solving the hydrodynamic field equations explicitly, we intend to extract this information directly from the ensemble of trajectories.

We assume that the quantum density can be represented by a mixture model^{13,14} determined by summing a finite number M of Gaussian components or “clusters.” The mixture model decomposition is expressed as a sum of joint probabilities

$$\rho(\mathbf{r}) = \sum_m^M p(\mathbf{r}, c_m), \quad (23)$$

where $p(\mathbf{r}, c_m)$ is the probability that a randomly chosen member of \mathcal{R} has the configuration \mathbf{r} and is a variant of the m th Gaussian cluster designated by c_m . Each Gaussian cluster is parametrized by a weight $p(c_m)$, a mean position vector $\boldsymbol{\mu}_m$, and a vector of variances $\boldsymbol{\sigma}_m^2$. We can also replace the variance vector with a full covariance matrix \mathbf{C}_m if necessary.

By definition,⁶⁰ each joint probability in Eq. (23) is related to a pair of conditional probabilities according to the relation

$$p(\mathbf{r}, c_m) = p(c_m)p(\mathbf{r}|c_m) = \rho(\mathbf{r})p(c_m|\mathbf{r}), \quad (24)$$

where the forward conditional probability $p(\mathbf{r}|c_m)$ refers to the probability that a randomly chosen variant of c_m has the configuration \mathbf{r} . Conversely, the posterior probability $p(c_m|\mathbf{r})$ refers to the probability that the configuration point \mathbf{r} is a variant of the cluster c_m . In probability theory the factors $\rho(\mathbf{r})$ and $p(c_m)$ are marginal probabilities; however, we shall simply refer to them as the quantum density and weight of the m th Gaussian cluster, respectively. The expansion weights are strictly positive semidefinite and sum to unity. Substituting the first equality of Eq. (24) into Eq. (23) we have

$$\rho(\mathbf{r}) = \sum_m^M p(c_m)p(\mathbf{r}|c_m), \quad (25)$$

where we can specify the form of $p(\mathbf{r}|c_m)$ to reflect our belief that $\rho(\mathbf{r})$ is a mixture of Gaussian components. We explore this approximation with two different Gaussian cluster models.

The first model assumes that each cluster is completely separable and takes the form of a product over the N_d -dimensional configuration space,

$$p(\mathbf{r}|c_m) = \prod_d^{N_d} \sqrt{\frac{1}{2\pi\sigma_{m,d}^2}} e^{-(r_d - \mu_{m,d})^2 / (2\sigma_{m,d}^2)}. \quad (26)$$

The second model explicitly takes into account nonseparable correlations in configuration space and incorporates the full covariance matrix,

$$p(\mathbf{r}|c_m) = \sqrt{\frac{\|\mathbf{C}_m^{-1}\|}{(2\pi)^{N_d}}} e^{-(\mathbf{r} - \boldsymbol{\mu}_m)^T \cdot \mathbf{C}_m^{-1} \cdot (\mathbf{r} - \boldsymbol{\mu}_m) / 2}. \quad (27)$$

In comparison with the separable case, the fully covariant model can represent more complicated density structures with fewer clusters; however, this is at the cost of greater computational expense. For low dimensional systems it is advantageous to use the fully covariant model, but in high dimensions it is much more efficient to use a larger number of separable clusters. The principle at work here is related to the idea of collective correspondence discussed by Heller⁶¹ regarding the cooperative effort of overlapping Gaussian wave packets to describe position-momentum correlations in phase space. It is also feasible to construct a mixture model that incorporates any combination of covariant and separable

degrees of freedom especially if there is reason to do so based on the symmetry of the physical problem.

B. Expectation maximization

Now that we have established a model to work with, the trick is to determine the Gaussian parameters $p(c_m)$, μ_m , and C_m (or σ_m). The mean position vector and covariance matrix of the clusters are defined by the moments of the forward conditional probabilities

$$\mu_m = \int \mathbf{r} p(\mathbf{r}|c_m) d\mathbf{r}, \quad (28)$$

$$C_m = \int (\mathbf{r} - \mu_m)^T (\mathbf{r} - \mu_m) p(\mathbf{r}|c_m) d\mathbf{r}. \quad (29)$$

For the separable case, the variances are given by the diagonal elements $\sigma_{m,i}^2 = (C_m)_{ii}$. Rearranging Eq. (24) and substituting into Eqs. (28) and (29), we can write these parameters as

$$\mu_m = \int \mathbf{r} \frac{\rho(\mathbf{r}) p(c_m|\mathbf{r})}{p(c_m)} d\mathbf{r}, \quad (30)$$

$$C_m = \int (\mathbf{r} - \mu_m)^T (\mathbf{r} - \mu_m) \frac{\rho(\mathbf{r}) p(c_m|\mathbf{r})}{p(c_m)} d\mathbf{r}, \quad (31)$$

which are easily approximated by a pair of Monte Carlo sums over the ensemble of de Broglie–Bohm particles,

$$\mu_m \approx \frac{1}{N p(c_m)} \sum_n \mathbf{r}_n p(c_m|\mathbf{r}_n), \quad (32)$$

$$C_m \approx \frac{1}{N p(c_m)} \sum_n (\mathbf{r}_n - \mu_m)^T (\mathbf{r}_n - \mu_m) p(c_m|\mathbf{r}_n). \quad (33)$$

A similar expression for the expansion weights in terms of a sum over \mathcal{R} is given by

$$p(c_m) \approx \frac{1}{N} \sum_n p(c_m|\mathbf{r}_n). \quad (34)$$

The posterior terms $p(c_m|\mathbf{r}_n)$ for each data point in Eqs. (32)–(34) are evaluated directly from the forward probabilities according to Bayes' formula,

$$p(c_m|\mathbf{r}_n) = \frac{p(c_m) p(\mathbf{r}_n|c_m)}{\sum_m p(c_m) p(\mathbf{r}_n|c_m)}. \quad (35)$$

In some sense, the ensemble of particles can be viewed as a data set that catalogs the results of many successive measurements on an ensemble of identically prepared quantum systems. Each member of the ensemble yields an equal amount of information describing the underlying probability distribution. The key to understanding how this information is distributed among the Gaussian clusters is contained within Bayes' formula. From a Bayesian viewpoint the numerator in Eq. (35) essentially reduces to a measure of how well the cluster c_m describes the fluid element with configuration \mathbf{r}_n . The sum in the denominator is a measure how well the particle at \mathbf{r}_n is described by all of the clusters. The ratio of the two quantities then determines the fraction of explanatory

information that the particle gives to the m th cluster. Hence the cluster which best describes \mathbf{r}_n will have the largest posterior probability for that point.

The circular structure in Eqs. (23)–(35) provides the framework for an iterative procedure known as the expectation-maximization (EM) algorithm^{13–15} that seeks to find a set of parameters that gives the best estimate for the density of \mathcal{R} . Computing the forward and posterior probabilities determines how well an arbitrarily parametrized mixture model is *expected* to represent the ensemble. Evaluating the sums in Eqs. (32)–(34) gives rise to a new set of parameters that is said to *maximize* the log-likelihood,

$$L = \ln \prod_n \rho(\mathbf{r}_n) \quad (36)$$

of the distribution. A likelihood is a probability measure referring to the outcome of an event that is already known to have occurred. The log likelihood of the distribution is a measure of how well the overall density model describes the whole collection of data points. The EM algorithm works very much like the variational principle, in that there is a likelihood equation defined over parameter space,

$$\nabla_{c_m} L = 0, \quad (37)$$

such that L is a maximum for models that are effective in describing the ensemble's distribution. Furthermore, it can be shown that the update rules in Eqs. (32)–(34) move the clusters through parameter space in the direction along $\nabla_{c_m} L$, that is, in the direction that improves the density estimate. The cycle of estimating the expected distribution function and maximizing the log-likelihood is repeated iteratively until a satisfactory estimate of the density is achieved.

It is important to realize that finding the maximum likelihood estimate of a distribution is not always a well-defined problem. In fact, there are generally multiple roots to the likelihood equation, and it is not necessarily guaranteed that there is a global maximum. While this is an important problem, our main concern here is simply to find an *acceptable* set of parameters that approximately represents the quantum density. However, one problem that we will need to address concerns the number M of Gaussian clusters used in the density estimate. For a Gaussian wave packet evolving in a parabolic potential field the answer is simple, but in general we will never really know how many clusters to use. When a wave packet bifurcates at a potential barrier, it will often develop complicated oscillations and nodal structures that are impossible to capture with Gaussians. Though there are statistical methods for “guessing” the number of components in a statistical data set, we do not incorporate them here. Instead, we simply try to use a minimum number of Gaussian clusters that gives reasonable results.

The overall scheme of the mixture model approximation and EM algorithm is as follows: First we generate the ensemble of probability fluid elements, usually a Gaussian density packet, via some appropriate sampling technique. The EM algorithm is initialized by choosing a set of parameters for a pre-set number of Gaussian clusters. Typically the initial clusters are given a uniform weight $p(c_m) = 1/M$. The mean position vectors are randomly selected from the do-

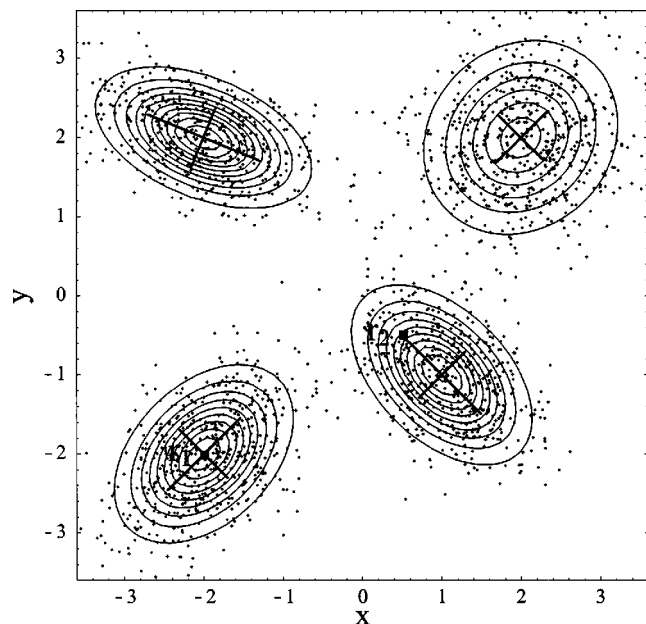


FIG. 1. The contours reflect a multivariate probability distribution comprised of four Gaussian components with nonzero xy covariances. The solid black lines represent the half widths of the Gaussian components. The ensemble of gray points are generated from the exact probability distribution function via a Metropolis sampling procedure and are taken as the input data for the EM algorithm. The black squares labeled r_1 and r_2 are tagged data points discussed later in Figs. 4 and 5.

main of the ensemble. The initial variances are chosen to be large enough to encompass the entire ensemble and the cross terms $(C_m)_{i,j}$ are zero. We cycle through the expectation-maximization routine until the parameters converge to an acceptable density estimate. Convergence can be evaluated in a number of ways by monitoring the cluster parameters, the conditional probabilities, the log-likelihood, or any combination thereof.

IV. COMPUTATIONAL RESULTS

A. Bivariate distribution with multiple nonseparable Gaussian components

To illustrate some of the points in the previous section, we demonstrate the convergence of the EM algorithm using a known probability distribution function. In Fig. 1 we have plotted the contours of a bivariate probability distribution function $\rho(x,y)$ consisting of four equally weighted nonseparable Gaussian components. The solid lines reflect the half width contours of each component and their orientation with respect to the x and y axes. The gray points correspond to an ensemble \mathcal{R} of 2000 variants of $\rho(x,y)$, which were randomly generated using a Metropolis sampling algorithm. Two of these data points, labeled \mathbf{r}_1 and \mathbf{r}_2 , have been tagged for later discussion.

In Fig. 2 we show the evolution of 16 separable Gaussian clusters over the course of the EM fitting algorithm. The contour plots indicate the relative intensity of the fitted density at various stages of the EM fit. The black dots and ovals correspond to the μ_m 's and σ_m contours for the individual Gaussian clusters. The initial random guess for the clusters is not illustrated. After one EM cycle, the clusters tend to ag-

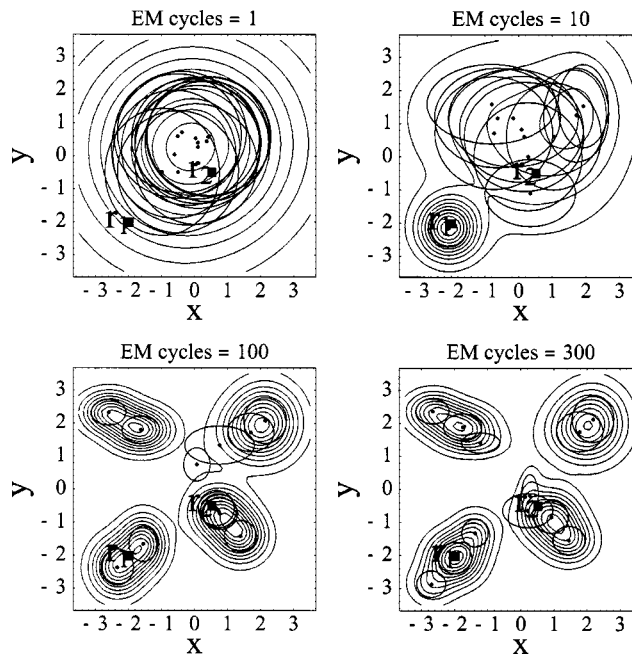


FIG. 2. This figure illustrates the EM algorithm for the data pictured in Fig. 1 using 16 separable Gaussian clusters. The contours reflect the approximated probability density during the course of the EM fitting routine. The black dots correspond to the average position of the Gaussian cluster, and the solid black ellipses represents the Gaussian half width contours.

gregate near the mean of \mathcal{R} , and the estimated density does not reflect any details of the exact distribution. After about ten EM cycles, the clusters begin sorting out the structure of the density. By 100 EM cycles, the clusters have found all four Gaussian components of the distribution and are struggling to recover the proper covariance in each component. The separable clusters are hindered in this because they have no freedom to rotate in the xy plane and must work collectively to capture the xy correlations. At 400 cycles we can see that the separable clusters have performed fairly well in finding the positions and relative orientations of the density components; however, the estimated density is somewhat distorted from the true distribution. The density estimate can be improved by including more sampling points and more clusters, but this also increases the computational demand.

Figure 3 illustrates the performance of the fully covariant model using four nonseparable clusters to describe the same data set. As expected, the fully covariant model performs much better than the separable case because the exact probability distribution is rigorously a mixture of four equally weighted nonseparable Gaussian components. After one EM cycle, the nonseparable clusters also collect near the mean of \mathcal{R} ; however, they immediately develop nonzero off-diagonal covariances. Between 10 and 20 EM cycles, the clusters locate the individual density components. By 50 cycles, the clusters have established have a stable configuration, which very closely mimics the true probability distribution.

Essentially, the EM algorithm performs a parallel search over the Gaussian parameter space and looks for regions where the clusters will be most effective in describing the data points. To help quantify the collective effort of the clus-

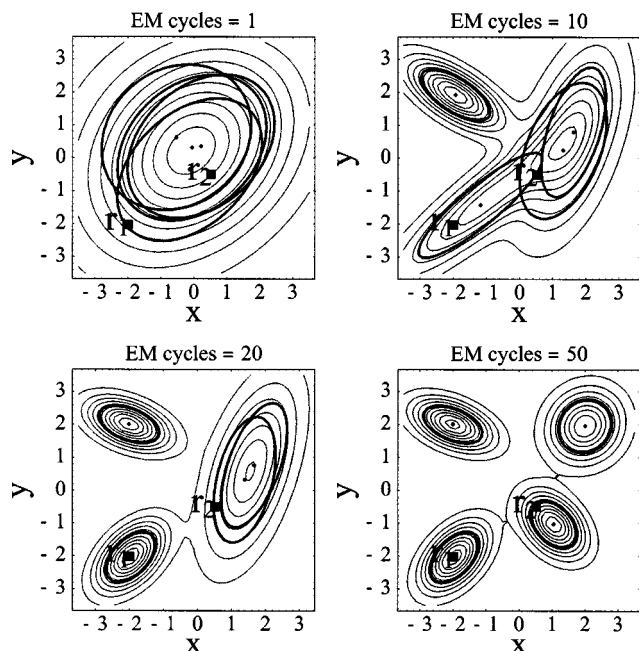


FIG. 3. This figure illustrates the EM algorithm for the data pictured in Fig. 1 using four nonseparable Gaussian clusters. Compared to the separable case, the fully covariant model gives much more accurate results with less clusters and fewer EM cycles.

ters, we examine the forward and posterior probabilities at the tagged data points \mathbf{r}_1 and \mathbf{r}_2 . First, notice in Fig. 2 that there is never more than one or two Gaussian clusters centered near the point \mathbf{r}_1 . Figures 4(a) and 4(b), respectively, show how the $p(\mathbf{r}_1|c_m)$'s and $p(c_m|\mathbf{r}_1)$'s evolve for the separable cluster model. Both plots indicate that for the first 75 EM cycles there is really only one cluster which dominates the density estimate at \mathbf{r}_1 . The posteriors are particularly

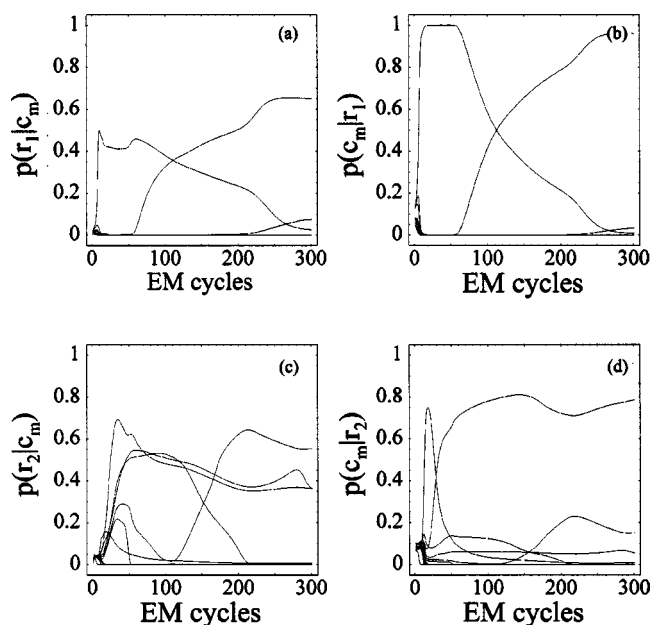


FIG. 4. Plot (a) shows 16 separable forward probabilities at the tagged data point \mathbf{r}_1 as a function of EM cycles. Plot (b) shows the corresponding posterior probabilities. Plots (c) and (d), respectively, depict the separable forward and posterior probabilities at the data point at \mathbf{r}_2 .

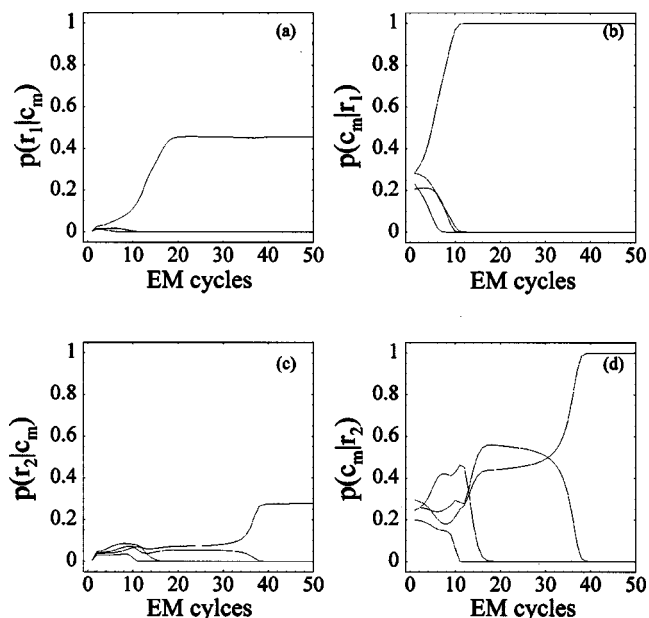


FIG. 5. Plot (a) shows four nonseparable forward probabilities at the tagged data point \mathbf{r}_1 as a function of EM cycles. Plot (b) shows the corresponding posterior probabilities. Plots (c) and (d), respectively, depict the four nonseparable forward and posterior probabilities at the data point \mathbf{r}_2 .

interesting because they reflect the fraction of explanatory power a data point gives to each of the cluster. The curve crossing at roughly 105 EM cycles reflects that the originally dominant cluster is eventually displaced by a different cluster that becomes nearly centered at \mathbf{r}_1 . The situation for \mathbf{r}_2 is analogous to that for \mathbf{r}_1 but is complicated by the fact that there is greater overlap between multiple clusters. The forward and posterior probabilities at the point \mathbf{r}_2 are shown in Figs. 4(c) and 4(d), respectively. Ultimately one cluster dominates the density estimate at \mathbf{r}_2 , however, this is to a lesser extent than at \mathbf{r}_1 .

In Fig. 5 we plot the forward and posterior probabilities at \mathbf{r}_1 and \mathbf{r}_2 for the fully covariant model. It is clear that the behavior of the nonseparable Gaussian clusters is consistent with the separable ones. The exception to this is that the fully covariant clusters converge to a stable configuration in fewer EM cycles. This point is highlighted by Fig. 6, where we plot the log-likelihood L for several different density fits. The separable cases are designated with a σ_m , where the integer m indicates how many Gaussians were used to perform the fit. Likewise, C_m refers to a fully covariant cluster fit with m nonseparable Gaussian components. The plateaus in the log-likelihood indicate that the EM algorithm is converging upon a root of the likelihood equation. It is conceivable that the EM algorithm could essentially become stuck at a local maximum or even a saddle point that does not give a particularly good density estimate. For these situations it is necessary to incorporate a small random perturbation in the cluster parameters in order move the fit away from such anomalous regions of parameter space. Another problem is that a cluster might become too focused on a single data point. This is described as a root of the likelihood equation lying on the exterior of parameter space. When this happens, the variance and weight of the cluster become exceedingly

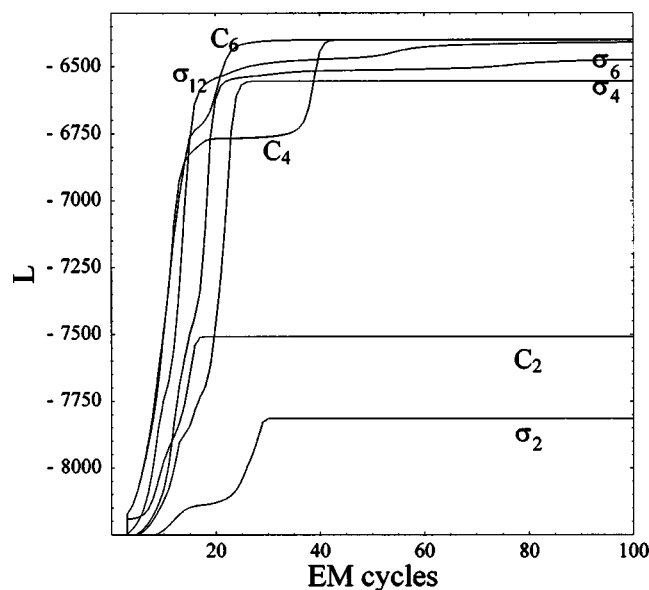


FIG. 6. Plot of the log-likelihood vs number of EM cycles for various density estimates of the data illustrated in Fig. 1. The notation σ_m and C_m refers to a density fit performed with m Gaussian clusters using the separable and fully covariant model, respectively.

small and in numerical applications will often round to zero, causing some terms in Eqs. (27) and (26) and (32) and (33) to diverge. This problem can be avoided in practice by adding a small fraction to the diagonal covariances in Eq. (33). This imposes an artificial boundary in parameter space that forces the Gaussian clusters away from the exterior roots.

B. Ground state of methyl iodide

Now that we have highlighted some key features of the mixture model approximation and EM algorithm, we turn our attention to a problem with more physical merits. In order to propagate the quantum ensemble in time we must compute both the classical and quantum forces acting on the ensemble particles. Given a maximum likelihood estimate for ρ in the form of Eqs. (26) or (27), it is a fairly straightforward exercise in bookkeeping to compute an approximate quantum force,

$$F_Q = \frac{\hbar}{4m} \left[\frac{\nabla^3 \rho}{\rho} - \frac{\nabla(\nabla \rho \cdot \nabla \rho)}{2\rho^2} - \left(\frac{\nabla^2 \rho}{\rho} - \frac{\nabla \rho \cdot \nabla \rho}{\rho^2} \right) \frac{\nabla \rho}{\rho} \right] \quad (38)$$

in terms of the Gaussian parameters. The quantum and classical forces are then used to drive the ensemble of trajectories by integrating Eqs. (16) and (17) over a short time step using a Verlet leapfrog-type method. The EM algorithm is repeated using the previously fit cluster parameters as the starting point. Recycling the old parameters significantly decreases the number of EM cycles required to obtain convergence in the next density estimate. The whole process of alternating between EM cycles and Verlet steps continues until we have integrated the equations of motion to some appropriate final time.

For a Gaussian density packet evolving on a parabolic potential surface, the mixture model approximation requires

only one cluster and is exact for all time. For nontrivial problems, however, the quantum density will generally exhibit a very complicated structure in configuration space. Clearly, the mixture model approximation will not be able to capture the exact intricacies of a realistic quantum distribution. Consequently, it is not feasible, using the present formulation of our methodology, to obtain numerically accurate quantum densities for nonstationary systems. Ground-state quantum densities, on the other hand, are characteristically much simpler than their excited-state and nonstationary counterparts. We believe our approach will be most useful for determining the ground-state properties of high dimensional systems.

For stationary systems the quantum force exactly counterbalances the classical force, and the ensemble of quantum trajectories does not evolve in time. The ground state can then be realized from a nonstationary state by adding a small damping term to Eq. (16),

$$\dot{\mathbf{v}} = F_Q - \nabla V/m - \gamma \mathbf{v}, \quad (39)$$

where γ represents a small dissipative coefficient. This fictitious friction, in turn, causes the ensemble particles to lose a small amount of kinetic energy at each time step in the simulation. For a classical ensemble, the distribution collapses to a delta function(s) centered about the minimum energy point(s) of the potential surface. For the quantum-mechanical ensemble, however, as the distribution becomes increasingly narrow, the quantum force becomes very strong and requires the ensemble to maintain some minimum finite width. At longer simulation times an equilibrium is reached, and the resulting distribution is representative of the ground-state quantum density. The corresponding ground-state energy can be resolved to within the statistical error of a Monte Carlo integration over the ensemble elements.

To illustrate this, we demonstrate the convergence of an initial Gaussian ensemble to the ground-state distribution for the $\text{CH}_3\text{-I}$ stretching/bending modes of the lowest electronic state of methyl iodide. For our purposes this provides a nontrivial anharmonic potential surface to test our methodology. The vibrational system is treated as a single particle ($m = 20\,000$ amu) evolving on a two-dimensional (2D) model potential-energy surface developed by Shapiro and Bersohn.⁶² The potential-energy curves for this anharmonic surface are depicted in Fig. 7 by the gray contour lines. In Fig. 7(a) we illustrate a numerically exact representation of the ground-state density obtained by diagonalizing the Hamiltonian of the system using a 2D discrete variable representation (DVR). The grid points indicate the minimum number of Chebychev quadrature points required to obtain convergence in the lowest energy eigenvalue. Obviously, a much larger grid would be necessary to perform a dynamical calculation on this system.

Figures 7(b) and 7(c) illustrate the estimated density for both the separable and fully covariant models, respectively. The black ovals represent the half width contours of the Gaussian clusters. There are four clusters in separable case and two for the fully covariant model. The various contour plots labeled (1), (2), and (3) correspond to snapshots of the estimated density at different points in the simulation. For both models, the initial density (1) is Gaussian, and all but

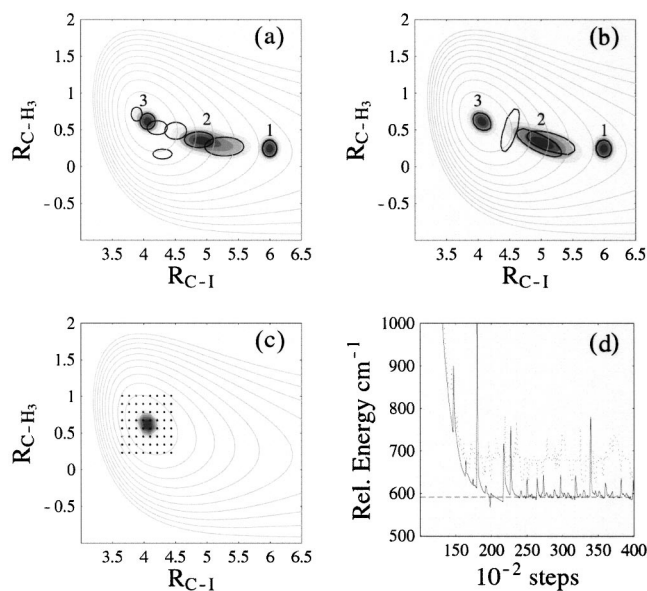


FIG. 7. Plots (a) and (b) show the relaxation of a Gaussian wave packet in an anharmonic potential well for both the separable and fully covariant models, respectively. The gray contours reflect the potential-energy curves for a model of CH_3I . The shaded contours indicate the shape of the approximated density after (1) 0, (2) 10 000, and (3) 40 000 Verlet time steps, respectively. The solid curves represent the half width contours of the Gaussian clusters. Plot (c) shows the numerically accurate DVR ground state and the associated grid of quadrature points. Plot (d) shows the energy of the estimated density as a function of time steps. The dotted and solid data correspond to the separable and nonseparable models, respectively, while the dashed horizontal line represents the DVR energy.

one of the clusters are redundant. As the ensemble is propagated the individual clusters behave differently from one another. The contours (2) show the quantum density at an intermediate time after roughly 10 000 Verlet time steps ($\delta t = 1$ atomic time unit). At longer times an equilibrium is achieved and the contours (3) are representative of the quantum ground state. In Fig. 7(d) we plot the energy of the system relative to the bottom of the potential well as a function of the number of Verlet time steps. The DVR energy at 591 cm^{-1} serves as a benchmark and is indicated by the dashed horizontal line. The dotted and solid energy curves are for the separable and nonseparable models, respectively. Dropping the first 20 000 time steps we find that the average energy for the separable case is $678.7 \pm 28.1 \text{ cm}^{-1}$, which is well above the DVR energy. The average energy for the nonseparable model falls within reach of the DVR energy at $600.6 \pm 24.1 \text{ cm}^{-1}$. The sharp energy spikes for the nonseparable calculation are due to anomalous changes in the cluster parameters such as a sudden jump in μ_m or rotation of \mathbf{C}_m . These effects do not pose a significant problem since the clusters quickly respond to correct the abnormalities within a few time steps. Filtering out these sporadic deviations improves the accuracy of the ground-state energy estimate and significantly reduces the statistical variation $593.5 \pm 4.8 \text{ cm}^{-1}$. For the sake of comparison we have also performed the same calculation for a mixture model with four fully covariant clusters. The average energy for the equilibrated system improves slightly $592.6 \pm 3.4 \text{ cm}^{-1}$; however, this is

at the cost of greater computational effort and slower convergence.

V. CONCLUSIONS

In this paper we have explored a new strategy for determining the quantum density associated with a statistical ensemble of de Broglie–Bohm space-time trajectories. Our methodology incorporates Bayesian probabilities and a mixture model approximation to calculate a parametrized estimate of Bohm's quantum force. The expectation-maximization procedure used to fit the density is not sensitive to trajectory crossings because the error associated with an individual rogue trajectory is essentially washed out by the statistical ensemble. Moreover, because the density fitting is formulated in terms of simple sums over data points, our method is easily extended to high dimensions and can be conveniently implemented on parallel computers.

Given a statistical ensemble of probability fluid elements, we can estimate the quantum force in terms of a set of Gaussian fitting parameters. Adding a small viscous drag to the equations of motion slowly removes excess kinetic energy from the system. After a sufficient equilibration time the ensemble is representative of the ground-state distribution and can be used to gather statistics on ground-state properties such as the zero-point energy and other expectation values. The approach we have described in this paper should be suitable for simulating the ground-state distribution of high dimensional vibrational systems such as weakly bound atomic and molecular van der Waals clusters. It may be worthwhile to investigate the use of Gaussian mixture models in connection with “smoothed” phase space distributions such as the Husimi distribution. Since Husimi functions are generally less complicated than the corresponding density matrices and Wigner functions, the mixture model approximation is expected to provide a more accurate representation of dynamical systems. Such a scheme could be used for examining mixed states and quantum dissipation in phase space. Another possibility is to employ higher-order clustering models that can account for more complicated functional dependence such as nodal structures. This may be useful for simulating vibrationally excited states, electronic densities, or calculating dynamical correlation functions. These topics will be addressed in future studies.

ACKNOWLEDGMENTS

This work was supported the National Science Foundation and the Welch Foundation. The authors would like to thank Professor Robert E. Wyatt for many helpful discussions and Dr. Sophia Garashchuk for graciously providing us with preprints.

¹P. M. Lee, *Bayesian Statistics: An Introduction* (Wiley, New York, 1997).

²W. Butine, *IEEE Trans. Knowledge Data Eng.* **8**, 195 (1996).

³J. C. Lemm, J. Uhlig, and A. Weiguny, *Phys. Rev. Lett.* **84**, 2068 (2000).

⁴J. C. Lemm and J. Uhlig, *Phys. Rev. Lett.* **84**, 4517 (2000).

⁵H. M. Wiseman, S. Mancini, and J. Wang, *Phys. Rev. A* **66**, 013807 (2002).

⁶C. M. Caves, C. A. Fuchs, and R. Schack, *Phys. Rev. A* **65**, 022305 (2002).

⁷A. M. Steinberg, *Phys. Rev. Lett.* **74**, 2405 (1995).

- ⁸A. N. Korotkov, Phys. Rev. B **63**, 085312 (2001).
- ⁹A. N. Korotkov, Phys. Rev. B **63**, 115403 (2001).
- ¹⁰A. N. Korotkov, Phys. Rev. A **65**, 052304 (2002).
- ¹¹D. F. R. Brown, M. N. Gibbs, and D. C. Clary, J. Chem. Phys. **105**, 7597 (1996).
- ¹²C. Huscroft, R. Gross, and M. Jarrell, Phys. Rev. B **61**, 9300 (2000).
- ¹³G. J. McLachlan and K. E. Basford, *Mixture Models: Inference and Applications to Clustering* (Dekker, Inc., New York, 1988).
- ¹⁴N. Gershenfeld, *The Nature of Mathematical Modeling* (Cambridge University Press, Cambridge, England, 1999).
- ¹⁵A. P. Dempster, N. M. Laird, and D. B. Rubin, J. R. Stat. Soc. Ser. B. Methodol. **29**, 1 (1977).
- ¹⁶R. P. Feynman and A. R. Hibbs, *Quantum Mechanics and Path Integrals* (McGraw-Hill, New York, 1965).
- ¹⁷L. de Broglie, C. R. Acad. Sci. Paris **183**, 447 (1926).
- ¹⁸L. de Broglie, Nature (London) **118**, 441 (1926).
- ¹⁹L. de Broglie, C. R. Acad. Sci. Paris **184**, 273 (1927).
- ²⁰D. Bohm, Phys. Rev. **85**, 166 (1952).
- ²¹D. Bohm, Phys. Rev. **85**, 180 (1952).
- ²²D. Bohm and B. Hiley, *The Undivided Universe: An Ontological Interpretation of Quantum Theory* (Routledge, New York, 1993).
- ²³P. R. Holland, *The Quantum Theory of Motion* (Cambridge University Press, Cambridge, England, 1993).
- ²⁴C. Leforestier *et al.*, J. Comput. Phys. **94**, 59 (1991).
- ²⁵J. C. Light, in *Time-Dependent Quantum Molecular Dynamics*, edited by J. Broeckhove and L. Lathouwers (Plenum, New York, 1992), p. 185.
- ²⁶R. E. Wyatt, J. Chem. Phys. **111**, 4406 (1999).
- ²⁷O. V. Prezhdo and C. Brooksby, Phys. Rev. Lett. **86**, 3215 (2001).
- ²⁸C. L. Lopreore and R. E. Wyatt, Phys. Rev. Lett. **82**, 5190 (1999).
- ²⁹E. R. Bittner, J. Chem. Phys. **112**, 9703 (2000).
- ³⁰E. R. Bittner and R. E. Wyatt, J. Chem. Phys. **113**, 8888 (2000).
- ³¹X. Oriols, F. Martín, and J. S. Suñé, Appl. Phys. Lett. **80**, 4048 (2002).
- ³²X. Oriols, J. J. García, F. Martín, J. S. Suñé, T. González, J. Mateos, and D. Pardo, Appl. Phys. Lett. **72**, 806 (1998).
- ³³E. Gindensperger, C. Meier, and J. A. Beswick, J. Chem. Phys. **113**, 9369 (2000).
- ³⁴E. Gindensperger, C. Meier, and J. A. Beswick, J. Chem. Phys. **116**, 10051 (2002).
- ³⁵E. Gindensperger, C. Meier, J. A. Beswick, and M. C. Heitz, J. Chem. Phys. **116**, 10051 (2002).
- ³⁶J. C. Burant and J. C. Tully, J. Chem. Phys. **112**, 6097 (2000).
- ³⁷R. E. Wyatt, C. L. Lopreore, and G. Parlant, J. Phys. Chem. **114**, 5113 (2001).
- ³⁸R. E. Wyatt and K. Na, J. Phys. Chem. **116**, 1228 (2002).
- ³⁹B. K. Dey, A. Askar, and H. Rabitz, J. Phys. Chem. **109**, 8770 (1998).
- ⁴⁰F. S. Mayor, A. Askar, and H. Rabitz, J. Phys. Chem. **111**, 2423 (1999).
- ⁴¹X. Hu, T. Ho, H. Rabitz, and A. Askar, Phys. Rev. E **61**, 5967 (2000).
- ⁴²Z. S. Wang, G. R. Darling, and S. Holloway, J. Chem. Phys. **115**, 10373 (2001).
- ⁴³I. Burghardt and L. S. Cederbaum, J. Chem. Phys. **115**, 10303 (2001).
- ⁴⁴I. Burghardt and L. S. Cederbaum, J. Chem. Phys. **115**, 10312 (2001).
- ⁴⁵J. B. Maddox and E. R. Bittner, J. Chem. Phys. **115**, 6309 (2001).
- ⁴⁶J. B. Maddox and E. R. Bittner, Phys. Rev. E **65**, 026143 (2002).
- ⁴⁷R. E. Wyatt and K. Na, Phys. Rev. E **65**, 016702 (2002).
- ⁴⁸T. J. Liszka, C. A. M. Duarte, and W. W. Tworzydło, Comput. Methods Appl. Mech. Eng. **139**, 263 (1996).
- ⁴⁹K. E. Hughes and R. E. Wyatt, Chem. Phys. Lett. **366**, 336 (2002).
- ⁵⁰C. Trahan and R. E. Wyatt, J. Chem. Phys. (to be published).
- ⁵¹S. Garashchuk and V. A. Rassolov, Chem. Phys. Lett. **364**, 562 (2002).
- ⁵²S. Garashchuk and V. A. Rassolov, J. Chem. Phys. **118**, 2482 (2003).
- ⁵³W. H. Miller, J. Phys. Chem. A **105**, 2942 (2001).
- ⁵⁴A. Donoso and C. C. Martens, Phys. Rev. Lett. **87**, 223202 (2001).
- ⁵⁵A. Donoso and C. C. Martens, J. Chem. Phys. **116**, 10598 (2002).
- ⁵⁶A. Donoso and C. C. Martens, Int. J. Quantum Chem. **90**, 1348 (2002).
- ⁵⁷E. P. Wigner, Phys. Rev. **40**, 749 (1932).
- ⁵⁸D. M. Ceperley and E. L. Pollock, Phys. Rev. Lett. **56**, 351 (1986).
- ⁵⁹B. L. Hammond, W. A. Lester, and P. J. Reynolds, *Monte Carlo Methods in Ab Initio Quantum Chemistry* (World Scientific, River Edge, NJ, 1994).
- ⁶⁰C. W. Gardiner, *Handbook of Stochastic Methods for Physics, Chemistry, and the Natural Sciences* (Springer-Verlag, New York, 1985), 2nd ed.
- ⁶¹E. J. Heller, J. Chem. Phys. **75**, 2923 (1981).
- ⁶²M. Shapiro and R. Bersohn, J. Chem. Phys. **73**, 3810 (1980).